

Creep mechanisms in quasi-plastic silicon nitride by instrumented indentation

František Lofaj

Institute of Materials Research of the Slovak Academy of Sciences, Watsonova 47, 043 53 Košice, Slovakia

Received 25 August 2005; received in revised form 9 November 2005; accepted 11 November 2005

Available online 6 January 2006

Abstract

Quasi-plastic creep behavior of the commercial, fine-grained silicon nitride grade, ST 1, was investigated using variety of techniques with the focus on the analysis of instrumented indentation. Creep deformation in this material was characterized by high creep rates at temperatures above 1300 °C and failure strains around 20%. It was accompanied by strong oxidation, cracking of the oxide layers, excessive cavitation at multigrain junctions and slight texture formation. Instrumented indentation revealed degradation of indentation moduli in the oxide layers and enhancement of oxidation and elastic moduli degradation during creep. Because of the similarities between the mass transport processes in cavitation, diffusion processes involved in oxidation and similar activation energies, both creep and oxidation occur simultaneously, however, oxidation is enhanced by external stress. Texture formation implied from disappearance of α -silicon nitride and anisotropy of indentation modulus contributes insignificantly (<5%) to total tensile strain. Creep processes in the studied material can be explained within the expanded cavitation creep model of Luecke and Wiederhorn assuming that cavitation is facilitated by low viscosity residual glass and small matrix grain size. Tertiary-like creep is attributed to the gradual increase of the applied stress resulting from the reduction of the effective cross section due to the formation of cracked oxide layers. Size and pre-oxidation effects were predicted and confirmed using creep samples with different gauge size.

© 2005 Elsevier Ltd. All rights reserved.

Keywords: Creep; Si₃N₄; Structural applications; Instrumented indentation

1. Introduction

Structural ceramics, including silicon nitride, became the subject of renewed interest because of improved price/performance ratio and reliability proven in successful applications, though mostly at room temperature.^{1–3} Silicon nitride ceramics is a class of materials with very wide range of mechanical properties. Creep resistance of different silicon nitride grades can vary at the same conditions by more than 5 orders of magnitude (Fig. 1).^{4–8} Even if the effects of grain size and morphology are considered, the most probable reason for such wide range of creep rates is related to chemical composition of the secondary phases. These phases originate from the sintering additives, typically oxides of Y, Yb or other rare-earth elements. They react with surface silica layer to form liquid phase during sintering. This liquid remains as a continuous amorphous phase at the grain boundaries after cooling. Intentional devitri-

fication partially reduces the amount of the amorphous phase and the grains of the crystalline secondary phases form at the multigrain junctions. However, approximately 1 nm thin residual glassy films always separate silicon nitride grains of the matrix as well as the grains of the crystalline secondary phases. The intergranular amorphous films (IGF) are the oxynitride glasses which contain rare-earth cations originating from the sintering additives. The properties of IGF and subsequently, the properties of the polycrystalline ceramics containing these films, are controlled by the type and amount of the additives and impurities.⁹

Fig. 1 compares temperature dependencies of the normalized creep rates at different temperatures in different silicon nitride grades. The substitution of Lu-containing additives instead of Y/Yb₂O₃ and earlier Al₂O₃ elimination combined with the additive amount reduction and better microstructure control resulted in significant increase in creep resistance.⁷ Assuming maximum allowable strain of ~1% in 10,000 h to be a critical design limit for rotor blades in a ceramic gas turbines,⁴ the strain rate of the material has to be $<3 \times 10^{-10} \text{ s}^{-1}$. Fig. 1 suggests that the maximum temperature allowed at a stress of 150 MPa is in SN 281

E-mail address: frantisek.lofaj@jrc.nl

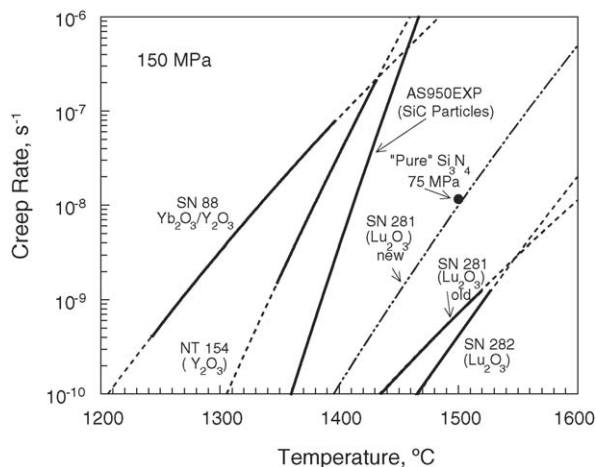


Fig. 1. A comparison of temperature dependence of tensile creep rates in different generations of silicon nitride ceramics under stress of 150 MPa.^{6–8} The plots for SN281 include earlier⁷ and the later data⁶ from different batches.

grade at least 50–100 °C higher than in the previous generation of silicon nitride containing only Yb and Y and up to 200 °C higher than in the grades containing Al.^{4–6,8}

Despite disadvantage of Al₂O₃ as sintering additive from the viewpoint of high temperature creep resistance, alumina additives are still often used because of several reasons. First of all, most of the current silicon nitride applications are at room or only elevated temperatures. Secondly, alumina is cheap and a very effective sintering additive for densification of silicon nitride and control of its microstructure. Another advantage is that it can form not only high refractory YAG (yttrium aluminum garnet) secondary crystalline phase but Al can be incorporated into silicon nitride to form SiAlON-s.¹⁰ Some of sialon properties, e.g. hardness and wear resistance, may exceed those of silicon nitride ceramics. Silicon nitride-alumina-yttria systems are also the most studied systems up to now. Due to the possibility of precise microstructure control, room temperature bending strength of numerous experimental and even some commercial materials, e.g. ST 1, exceeds 1 GPa.^{11–13} High strength of this material retains up to almost 1200 °C, however, rapid degradation occurs at higher temperatures. Our earlier creep studies on this grade at the temperatures above 1300 °C revealed unusual creep behavior with the failure strains exceeding 20% during the prolonged accelerated stage.^{13–16} They were accompanied by intensive cavitation in the core, strong oxidation enhanced by stress in surface layers and intensive cracking of these layers.¹³ The obtained strains were up to five times higher than those in the standard silicon nitride grades,^{17–20} however, at least half order of magnitude lower than the strains obtained during superplastic deformation.²¹ Superplastic deformation is usually observed at temperatures above 1500 °C in inert atmosphere when cavitation is suppressed.^{21,22} The effects related to oxidation seem to cause the deformation in the nano-sized silicon nitride to be significantly different from that at lower temperatures, as well as from that of conventional creep resistant ceramics and from superplastic deformation. To distinguish such transitional behavior between creep and superplasticity, the terms “quasi-plasticity” or “quasi-ductile” behavior were suggested for this type of

material.^{13–16} However, though cavitation was considered to be the most important for producing large strains, the interaction between oxidation and creep was not fully understood.

Strong oxidation accompanying creep in ST1 prevents using conventional methods, such as density change measurements^{9,23,24} and ultrasonic methods^{25,26} for the study of the creep mechanisms. However, instrumented indentation seems to be suitable method because it is extremely localized in comparison with the thickness of the oxidation affected zones and simultaneously, the studied volume is sufficiently large to contain information about the processes in the material.²⁶ This method was already successfully used for creep cavitation studies in another silicon nitride grade, where oxidation was negligible.^{25,26} The interpretation of indentation data was straightforward in this material and the changes in microhardness and elastic moduli were directly related to the extent of cavitation.^{25,26} However, the correlation is not simple when strong oxidation overlaps with creep deformation and cavitation. The progress in understanding cavitation creep allows us to incorporate oxidation and other effects into quasi-plastic creep model at least at qualitative level.^{8,24} Thus, the aim of the work is to elucidate possible tensile creep mechanisms in quasi-plastic silicon nitride including oxidation and other effects with the emphasis on the analysis of the data obtained by instrumented indentation.

2. Experimental procedure

2.1. Material characterization

The studied material was the commercial grade of silicon nitride designated as ST 1 (NGK Spark Plug Co., Ltd., Japan) designed for high strength components operating at temperatures below 1300 °C. Its microstructure consists of fine β -Si₃N₄ matrix grains with the mean diameter of ~ 0.2 μ m, aspect ratio 2–4, and of a small amount of larger reinforcing grains with the length up to 5 μ m and a diameter of 0.3–0.5 μ m. Secondary phases contained Yb and Al. X-ray showed the presence of small amount of α -Si₃N₄ besides β -Si₃N₄ as major phases and Yb₂Si₂O₇ and others as minor phases. The average strength in 4-point bending mode (30 mm/10 mm) at room temperature was 1085 MPa and the fracture toughness 6.5 and 5.8 MPa m^{0.5} measured on single-edge notched beam and single edge precracked beam samples (JIS R 1607), respectively.^{13–16}

2.2. Creep testing

Tensile creep testing. The tests were performed on two types of the dog-bone shaped specimens with a rectangular cross section (2.5 mm \times 4 mm) and gauge lengths of 20 and 18 mm, respectively, and on larger button-head samples with the circular cross section (diameter—6 mm, gauge length—35 mm). The sections cut from the integrated flags of dog-bone specimens were used as a reference to compare the effects of oxidation and creep. Dog-bone shaped samples were crept on creep machines with lever arm and SiC hot grips in air at the temperatures from

1200 to 1450 °C under the applied stresses from 30 to 260 MPa. Button head samples were tested using universal testing machine and constant load. Specimen geometry, creep machines and testing procedure were described earlier.^{13–16,25–27}

Microstructure Study. Creep introduced changes in the microstructure were studied by light and scanning electron microscopy (SEM) on polished cross sections, creep fracture surfaces and secondary fracture surfaces obtained by intentional fracture of the samples after testing at room temperature. The changes in the phase composition were investigated by X-ray diffraction (XRD) and several foils were investigated by transmission electron microscopy (TEM).

Instrumented indentation. The distributions of the microhardness and indentation modulus were studied by the microhardness tester with the controlled load (Model H100 VP, Fischer, Germany) on the series of indents performed along the lines normal to the surface on the polished cross sections cut in the directions perpendicular and parallel to the applied stress. The load of 300 mN on Vickers indenter was applied in 60 steps with dwell time of 1 s at each step. The same conditions were used during unloading. Indentation modulus, $E_i = E/(1-\nu^2)$ (E is Young's modulus and ν is Poisson's constant) is determined from the unloading part of the indentation curve as $E_i = E/(1-\nu^2) = [dP/dh]/(1.142S_{max}^{0.5})$, where $[dP/dh]$ is the initial slope of the unloading curve (P is load and h is penetration depth) and S_{max} is the projected area of the indentation.²⁸

3. Results

3.1. Creep behavior

Creep behavior of the studied material depended strongly on the testing temperature. In the temperature range below 1300 °C, it was similar to the usual creep behavior in brittle ceramics: primary creep and prolonged secondary-like stages were followed by creep rupture without any accelerated stage. Failure strains in these cases were less than 5%. Creep behavior at temperatures above 1300 °C changed and it became similar to the behavior of ductile materials. Fig. 2 illustrates this case in the terms of

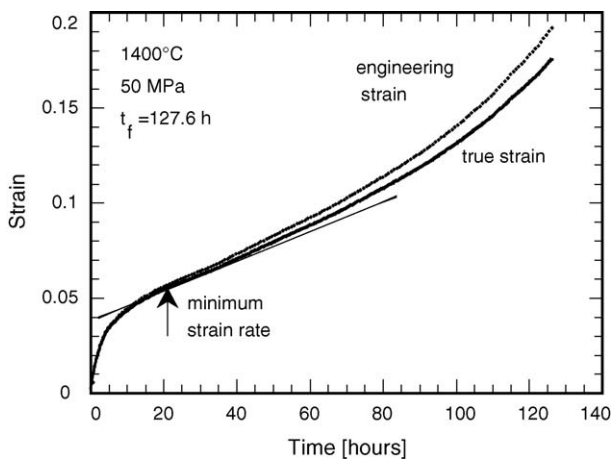


Fig. 2. Creep curves in ST 1 silicon nitride during tensile creep at 1400 °C indicate unusually large tensile strains obtained during extensive tertiary-like stage.^{13–15}

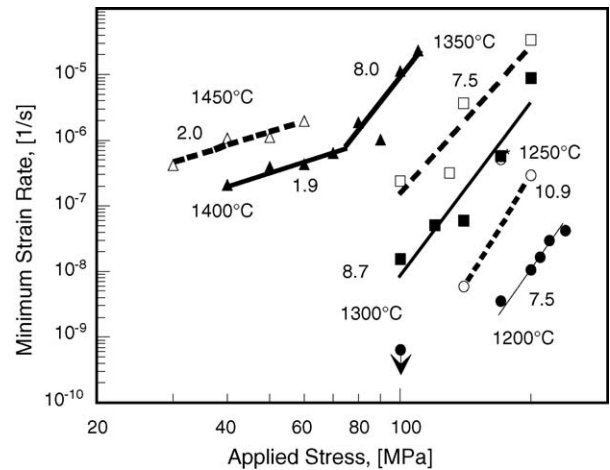


Fig. 3. Stress dependence of the minimum creep rates in ST 1 ceramics.^{13–16}

engineering strain $\varepsilon = \Delta l/l_0$ and true tensile strain, $\varepsilon_t = \ln(l/l_0)$, obtained at 1400 °C under the stress of 50 MPa. Both curves are composed of primary stage, short intermediate stage with a minimum strain rate and a prolonged accelerated stage. Despite such a large deformations, the difference between both curves is quite small. Therefore, only engineering strain will be considered throughout the work.

Total creep strain at 1400 °C reached nearly 20%, which is almost one order of magnitude greater than in other grades. The relationship between minimum strain rate and applied stress at different temperatures is shown in Fig. 3 in the dependence assuming power law behavior. A transition from relatively low stress exponents of about 2 to the exponents from 6 to 11 was observed at about 70 MPa in temperature range 1400–1450 °C. The apparent activation energy of creep was in the range 710–750 kJ/mol at relatively low stresses and high temperatures, and 920–1100 kJ/mol at high stresses and lower temperatures.

3.2. Microstructure studies

Visual observation of specimen surfaces did not reveal any oxidation related effects even after 7700 h long creep test at 1200 °C. However, whitish surface layer containing numerous large cracks and several thick subsurface layers formed during testing at temperatures above 1300 °C (Fig. 4(A)). Oxidation effects were significantly enhanced at the tips of those large cracks, which penetrated subsurface layers (see arrows in Fig. 4(A)). Although the size of these cracks sometimes exceeded 1 mm, which is considerably greater than critical crack size in brittle ceramics in the studied stress range, they not always caused failure. The morphology of the fracture surface in Fig. 4(B) suggests that fracture originated from a creep damage zone in the core zone of the specimen, which is outside of surface layers with very large crack in the sample corner.

Fig. 5(A) demonstrates polished gauge cross section oriented perpendicular to the applied stress whereas Fig. 5(B) shows a cross section cut from the unstressed flag of the same sample. Obviously, layer formation in later case resulted from oxidation.

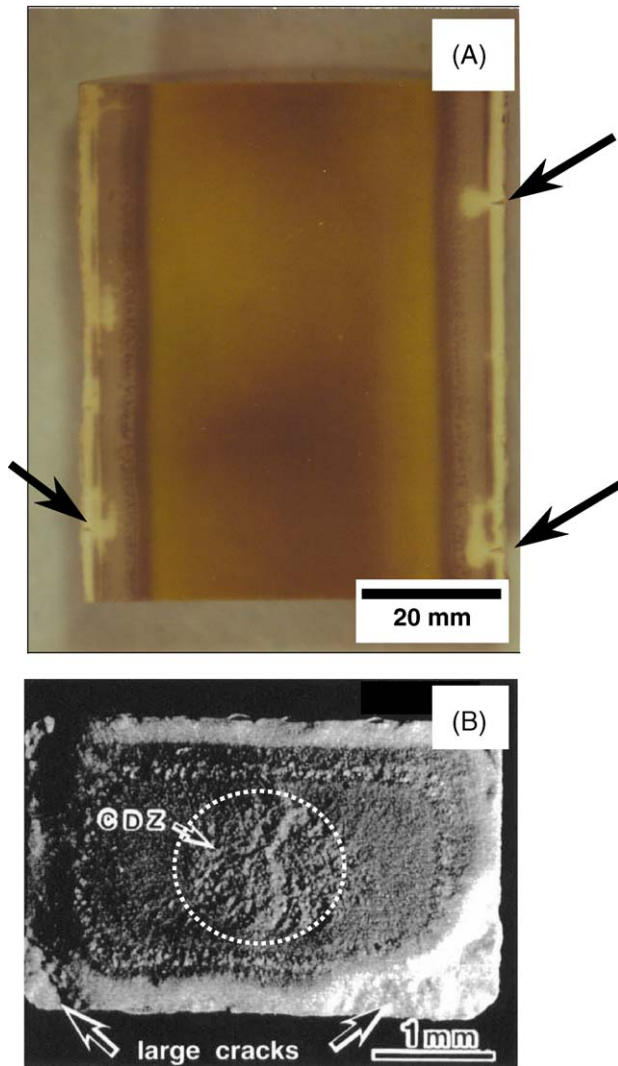


Fig. 4. (A) Surface and subsurface layers on a section cut parallel to the applied stress from the button-head sample after test at 1400 °C for 271 h under stress of 70 MPa. Layer formation was attributed to oxidation whereas the formation of numerous small and large cracks in these layers results from deformation. Arrows indicate enhanced oxidation at the tips of several large cracks, which penetrated subsurface layers. (B) Creep fracture surface of the sample tested at 1400 °C suggests that fracture originated from a creep damage zone (CDZ) in the core zone rather than from large surface cracks.

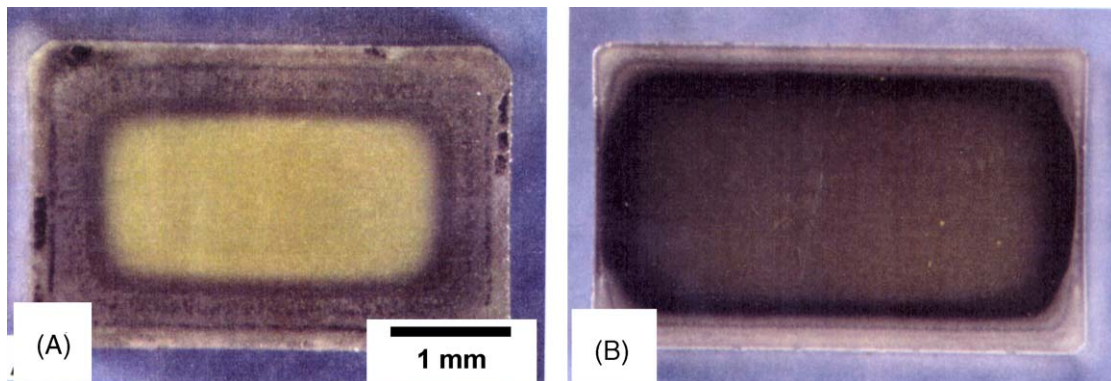


Fig. 5. (A) The cross section of the gauge zone after creep at 1400 °C for 84.8 h under stress of 70 MPa in air revealed formation of thick subsurface layers; (B) the cross section of the flag oxidized at identical conditions.

The layer thickness formed during creep (Fig. 5(A)) was more than twice greater than that after oxidation. Thus, applied stress resulted not only in creep deformation but also in enhancement of the oxidation processes. Moreover, and despite it is not visible on black and white micrographs, the color of the samples in the core changed from originally black to yellow after creep while it remained dark green in the flag. Such color changes implied that the whole volume of the sample was affected during creep.

Several sub-layers can be visually distinguished on both cross sections in Fig. 5. Electron microscopy investigation combined with the X-ray diffraction analysis revealed that the white surface layer consists of large elongated grains of $\text{Yb}_2\text{Si}_2\text{O}_7$ with the mean diameter up to 3 μm embedded in the amorphous, likely silica phase. The first, thin, light brown subsurface layer in Fig. 5(A) is almost pure $\beta\text{-Si}_3\text{N}_4$. Precipitates in the following layers were identified as $\text{Yb}_4\text{Al}_2\text{O}_9$. The crystalline secondary phases in the core zone of the specimen, besides $\beta\text{-Si}_3\text{N}_4$, were not identified. However, their composition is different from the initial composition (Fig. 6). Note that $\alpha\text{-Si}_3\text{N}_4$ phase, which was present in the as-received material, disappeared in the crept material. The possibilities of a solution of $\alpha\text{-Si}_3\text{N}_4$ phase, its re-precipitation as β -phase and texture formation were indicated by a change in the relative intensities of the diffraction peaks corresponding to the orientations $\langle 200 \rangle$ and $\langle 210 \rangle$ versus $\langle 101 \rangle$. The intensities of $\langle 200 \rangle$ and $\langle 210 \rangle$ increased while $\langle 101 \rangle$ peak intensity decreased after creep in comparison with the same peaks after oxidation (Fig. 7).

TEM observation of the samples prepared from oxidation affected subsurface layers and core zone of the sample revealed unusually high concentration of cavities: the microstructure was almost like a sieve (Fig. 8(A)) while no cavities were present in the grip zone (Fig. 8(B)). All cavities were multigrain-junction cavities, no other type was found. The size of these cavities was comparable to the size of matrix grains, which is less than 200 nm.

3.3. Instrumented indentations profiles

The changes of the microhardness and indentations modulus due to creep and oxidation were investigated on the cross sections of the gauges and undeformed flags or grips. The mean

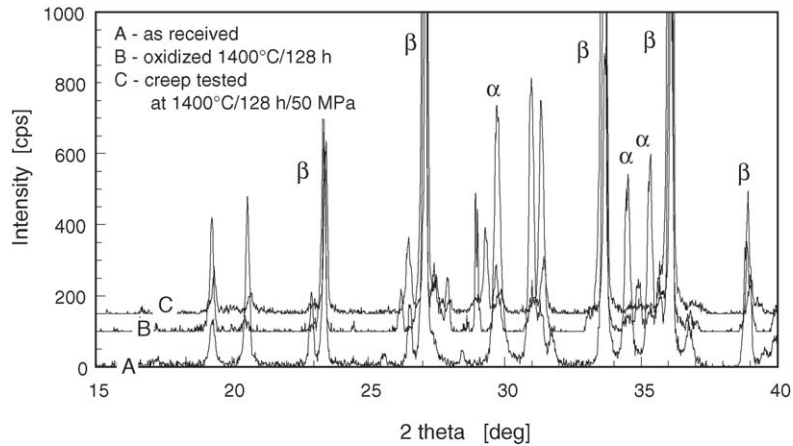


Fig. 6. X-ray diffraction patterns from the core zones of the as-received, crept and oxidized materials revealed changes in both secondary phases and silicon nitride matrix.

values of the indentation modulus and microhardness in the as-received material were 359 ± 11 GPa and $12,450$ N/mm², respectively. However, they varied among different subsurface layers after creep. The dependencies of the absolute values of the indentation modulus and microhardness on the distance from the surface are illustrated in Fig. 9. Microhardness varied from 5000 N/mm² up to $10,000$ N/mm², the indentation modulus from 160 to 310 GPa but both parameters exhibit very similar depth profiles. Microhardness and indentation moduli values correlated with the individual subsurface layers visually identified on the cross sections. The largest degradation of the microhardness and indentation modulus occurred in the

surface layer, considerably higher values were in the following additive free zone, and a drop followed by a gradual increase can be seen in the subsequent precipitate-containing layers. The yellow core had the highest and approximately constant microhardness and indentation modulus. However, both values were approximately 10% lower than in the as-received state.

Five profiles in Fig. 10 can be used to estimate the influence of creep conditions on indentation moduli profiles. Although temperatures varied from 1200 °C up to 1450 °C, and the lifetime was from 12748 to 37.5 h, respectively, the degradation profiles were similar. The values of indentation moduli in the core of the specimens were in a range from 73 to 83% of the initial values. When the standard deviation of the measurement of $\pm 3\%$ is considered, the final degradation seems to be in the range from 75 to 80% at each condition. The main differences between the profiles are in the subsurface zone. The decrease is more pronounced and the thickness of the layers with low elastic moduli is larger at higher temperatures. At 1200 °C, this zone was less than 200 μm thick while at 1450 °C it was almost 500 μm .

Fig. 11 shows relative indentation moduli distributions after creep at 1450 °C on the cross sections oriented parallel and perpendicular to tensile stress. The decrease of the indentation moduli on axial section was $\sim 22\%$ and around 25% on radial section. The differences between both distributions are $3\text{--}5\%$ in terms of elastic properties and around 100 μm in affected zone thickness. Although standard deviations are comparable with the differences between the obtained values, the data from axial section are systematically lower than those from the radial section. Thus, the difference originates from the material properties, most probably, from preferred orientation of silicon nitride grains after deformation. However, an attempt to visualize texture by using Electron Backscatter Diffraction (EBSD) technique was not successful due to very small matrix grain size.

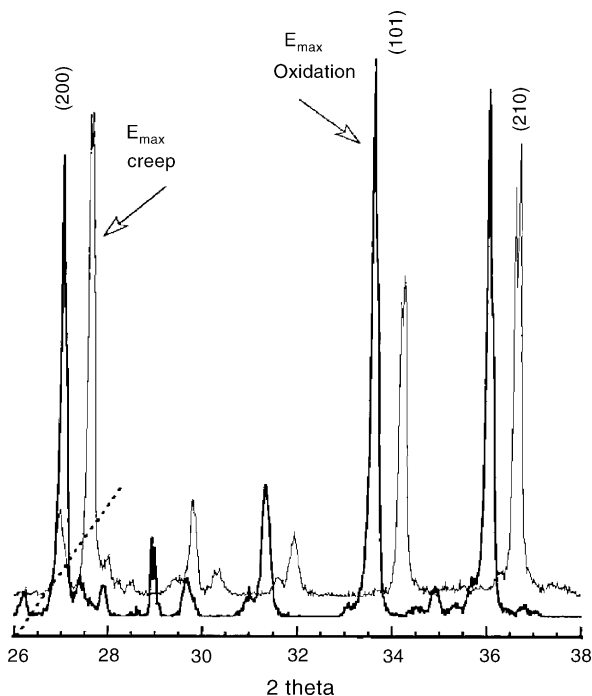


Fig. 7. A detail from Fig. 6: the changes in intensity ratio between (200) and (210) and (101) peaks of $\beta\text{-Si}_3\text{N}_4$ after creep indicates slight grain reorientation. The disappearance of $\alpha\text{-Si}_3\text{N}_4$ suggests the presence of solution-precipitation of silicon nitride.

4. Discussion

The results of microstructure studies and indentation profiles emphasize differences between quasi-plastic creep behavior, highly creep resistant silicon nitride grades and superplastically

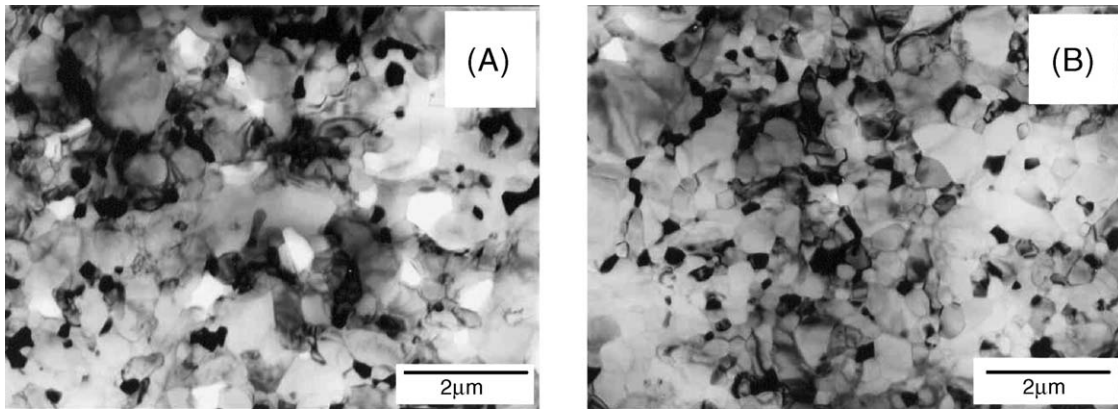


Fig. 8. A comparison of the microstructure after creep (A) and oxidation (grip) (B) at 1400 °C for 127.6 h under stress of 50 MPa ($\epsilon \sim 19\%$). Gauge zone of the sample is heavily cavitated and only multigrain junction cavities are present, whereas no cavitation is present in the grip.

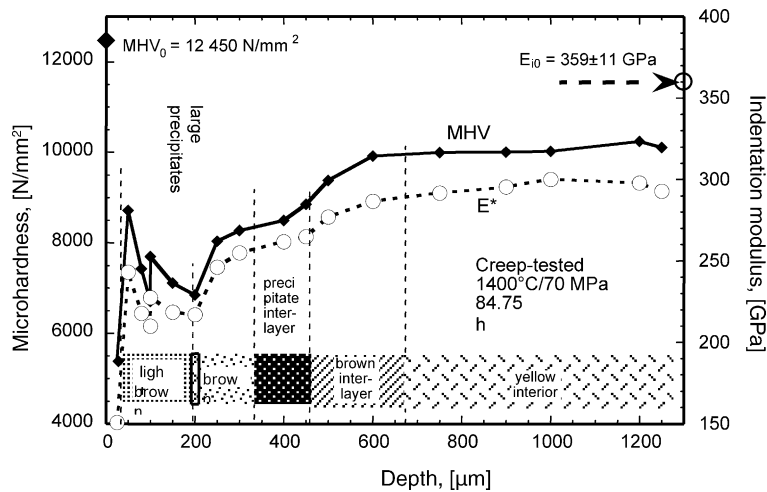


Fig. 9. The distributions of the indentation modulus and microhardness on the cross-sections perpendicular to the applied stress. The changes in profiles of both properties correlate with different subsurface layers. Each point corresponds to the average of five measurements. Standard deviation of the measurements was around 3%.

deformed grades as well. In conventional silicon nitrides, cavitation at multigrain junctions generates the main contribution to tensile strain^{8,14,23,24,27} whereas grain rearrangement accommodated by strong solution-precipitation (S-P) of silicon nitride with small contribution of cavitation is rate controlling during

superplastic deformation.²⁹ Relatively large strains accompanied by very intensive cavitation, strong oxidation effects resulting in elastic properties degradation, solution-precipitation of silicon nitride and a weak texture formation have to be built-

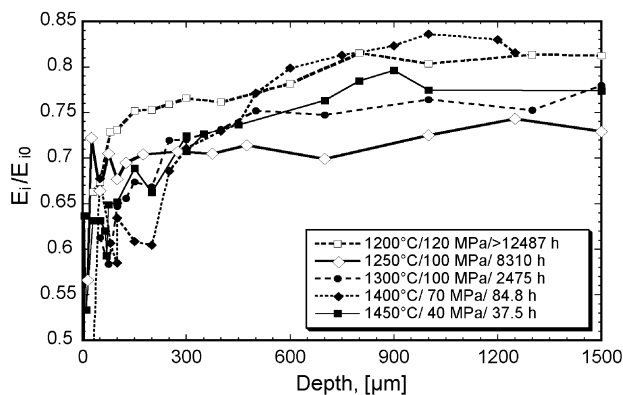


Fig. 10. A comparison of the relative indentation moduli profiles after creep at different conditions.

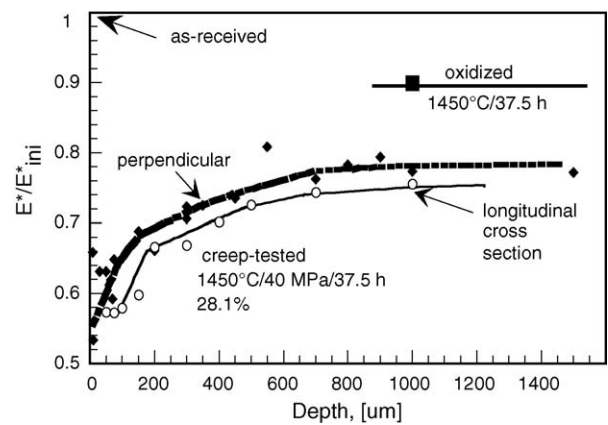


Fig. 11. Systematic differences between the indentation moduli profiles on the cross-section oriented parallel and perpendicular to the stress imply anisotropy of the indentation modulus due to preferred orientation of silicon nitride matrix.¹⁵

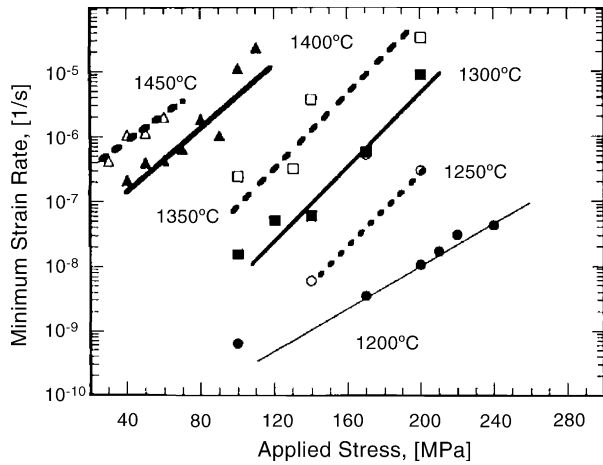


Fig. 12. Stress dependence of the minimum strain rate from Fig. 3 replotted according to the cavitation creep model of Luecke and Wiederhorn.²⁴

in the model of quasi-plastic creep behavior of the studied material.

4.1. Cavitation and quasi-plastic creep

Unusually high cavity concentration in the absence of visible silicon nitride grain growth and grain reorientation implies that cavitation plays significant role in quasi-plastic deformation similarly as in many other vitreous bonded ceramics. This assumption is supported by strain rate–stress dependence in Fig. 12, which assumes exponential dependence according to the cavitation creep equation suggested by Luecke and Wiederhorn²⁴:

$$\frac{d\varepsilon}{dt} = A\sigma \exp\left(\frac{-Q_c}{RT}\right) \left(\frac{f^3}{1-f^2}\right) \exp(\beta_c\sigma), \quad (1)$$

where A is a constant, f is the volume content of the secondary phase, β_c is a constant related to cavity nucleation, Q_c is the activation energy and σ is the stress. The change of stress exponent seen in Fig. 3 disappeared and all the data can be described using just one set of parameters. Such a good agreement between the experimental data and model indicates that cavitation can be the main creep mechanism even in the case of strains exceeding 20%. Strain rates in this material are, however, around 4–5 orders of magnitude greater than in other silicon nitrides in Fig. 1. Cavitation creep model has to be able to explain even such a difference in creep rates. According to the model,²⁴ cavitation at multigrain junctions is equivalent to the emptying multigrain junctions. It occurs via solution-precipitation of secondary phases (not S-P of silicon nitride) between multigrain junction pockets via residual glassy films. The presence of Al in the residual glass reduces its softening and melting temperatures, viscosity and increases diffusivity of the corresponding species in comparison with the residual glass without Al. Another important factor enhancing cavitation is the reduction of diffusion distance between the pockets due to smaller matrix grain size. Nano-sized matrix simultaneously enhances grain boundary sliding, which is necessary for cavity nucleation. Viscous flow of the residual glass is enhanced not only because

of higher homologous temperatures but also because of greater surface/volume ratio in very fine matrix. Thus, all the processes involved in cavitation creep in the nano-sized matrix with low viscosity glassy phase would be enhanced. Although an exact quantitative calculation is difficult, cavitation model can qualitatively accommodate considerably greater creep rates measured in ST 1.⁸

Cavitation creep model and many other creep models are derived from steady-state or minimum strain rate. This stage occurs relatively early in ST 1 and therefore, none of these models can account for oxidation at later stages. To avoid change in mechanism during creep, our very first approach adopted the idea of the same creep mechanism during the whole deformation.¹³ Based on the blunted tips of the cracks in the oxide layers it was assumed that the oxidation layers are so weak that they are not able to carry a load. Extensive tertiary-like creep (see Fig. 2) would result only from gradual reduction of the effective cross section of the gauge, which is equivalent to gradual increase of the applied tensile stress. Simple mathematical calculation showed that stress increase follows the shape of the extended tertiary stage on the creep curves.¹³ Thus, cavitation creep may be the main mechanism during the whole deformation regardless of oxidation effects at later stages.

4.2. Anisotropy and environmental effects

The above assumption of one permanent creep mechanism is suitable but rather oversimplified macro-scale approach. It neglects silicon nitride anisotropy (Figs. 7 and 11), stress enhanced oxidation (Fig. 5) and especially, gradual changes in residual glass composition, which inevitably accompany oxidation. An attempt to account for all these effects on micro-scale is made based on the detail understanding of the mechanisms involved in cavitation creep.

Cavitation creep in silicon nitride occurs via cyclic combination of grain boundary sliding, viscous flow and solution-precipitation redistribution of the crystalline secondary phase among the multigrain junctions.^{8,14,24,27} The redistribution of silicon nitride via S-P mechanism usually generates negligible contribution into the resulting creep strain and it was necessary only to produce intragranular cavities inserted in SN 88 grade.^{30,31} This is not the case in ST 1. Solution-precipitation of silicon nitride is required for the reorientation of the silicon nitride matrix grains toward $\langle 210 \rangle$ (Fig. 7) and to explain anisotropy of the elastic moduli. Moreover, it is directly implied from α - Si_3N_4 disappearance (Fig. 6), because α - Si_3N_4 to β - Si_3N_4 transformation can happen only via solution-precipitation. The contribution of S-P of silicon nitride is enhanced by a small size of the matrix grains and low viscosity of the residual glass as discussed earlier. However, the separation of the contribution of S-P of silicon nitride from contributions of the other mechanisms is difficult without quantitative measurement of grain reorientation. It should be quite low because it cannot even be recognized on the electron microscopy images. Fig. 11 provides additional indirect estimation. The difference between the effective elastic moduli in radial and axial direction is from 3 to 5%. Subsequently, the contribution of grain

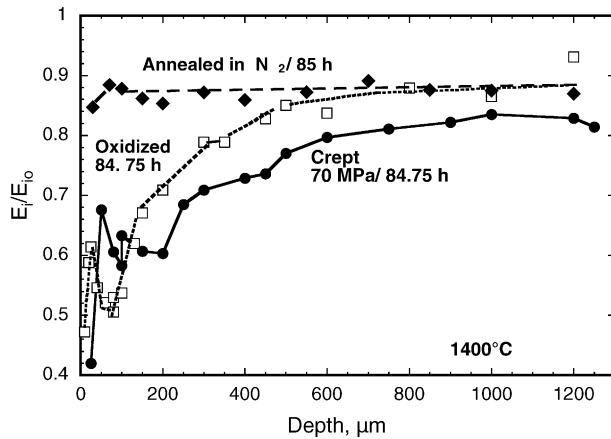


Fig. 13. The effect of heat treatment in nitrogen, air and creep on instrumented indentation profiles in ST 1 silicon nitride.

re-orientation driven by phase transformation and applied stress via S-P of silicon nitride to total tensile strain is expected to be in the same range, that is below 5%. Thus, in agreement with our earlier conclusion, quasi-plastic creep seems to result from cavitation creep with minor contribution of S-P of silicon nitride.

The composition and properties of the residual glass at the grain boundaries play crucial role in all processes involved in creep deformation of vitreous bonded ceramics and control creep resistance of the material.^{7–9} Residual glass films constitute also the main diffusion path for oxidation. However, residual glass properties can be affected by additional devitrification or any interaction within the secondary phases. Obviously, additional experiments involving only heat treatment are necessary to separate such effects from oxidation.

As-received ST-1 material was annealed in flowing nitrogen at the same conditions as in the case of oxidation and creep tests. The indentation moduli profiles obtained from the N₂-annealed, oxidized and crept samples are compared in Fig. 13. Heat treatment in nitrogen caused around 10% decrease of the indentation modulus. No visible or detectable layers formed in the subsurface zone in nitrogen atmosphere and indentation modulus decrease degradation was homogeneous across the whole volume. Oxidation for 85 h at 1400 °C resulted in more than 50% degradation of the indentation modulus at the surface and its gradual increase up to 90% of the initial value and convergence with the N₂ annealing profile approximately 700 μm below the surface. The profile of the crept sample was similar to that after oxidation but it was shifted to 20% degradation in the core and saturation was reached around 1000 μm under the surface. Thus, applied stress enhanced oxidation related decrease of the indentation modulus approximately twice and thickness of the corresponding layers by around 40%.

The possible mechanisms and processes accompanying quasi-plastic deformation are schematically summarized in Fig. 14. Homogeneous decrease of indentation modulus after annealing in nitrogen may result only from secondary phase evolution, most probably from additional devitrification and/or subtle changes within IGF/multigrain junction pockets, because silicon nitride grains can hardly be modified at these temperatures. The driving force for the changes could be only the devi-

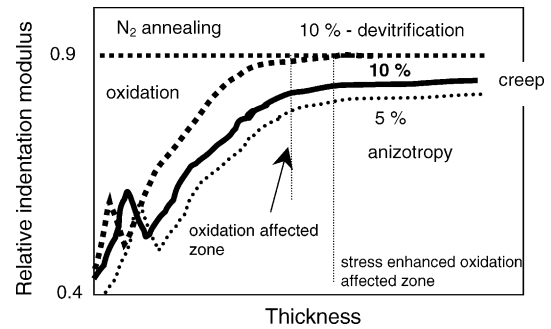


Fig. 14. Schematic analysis of the processes involved in the degradation of the indentation moduli in the studied silicon nitride during quasi-plastic deformation.

ation of the system from equilibrium state after relatively rapid cooling from sintering temperature. However, special study well beyond the scope of current work is necessary to identify such changes properly.

The profiles of the elastic properties degradation result from the penetration of oxygen from the surface and redistribution of the additives toward the surface. Our earlier studies found out that Yb and Al concentrations correlate with individual layers.^{13–16} The concentration of Al increased in the zone from 30 to 100% of total thickness of the oxidation affected zone compared to the bulk, whereas Yb concentration was lower there with the exception of large precipitates of Yb₄Al₂O₉. Sucking Yb and Al onto the surface resulted in a formation of the first, thin, porous subsurface layer composed from almost pure silicon nitride. This zone corresponds to the local peak in indentation modulus profile. The weight gain during oxidation increased according to parabolic law with the kinetic coefficients of $4.8 \times 10^{-12} \text{ mg}^2 \text{ s}^{-1} \text{ mm}^{-4}$ at 1300 °C, $4.1 \times 10^{-11} \text{ mg}^2 \text{ s}^{-1} \text{ mm}^{-4}$ at 1350 °C, and $1.4 \times 10^{-10} \text{ mg}^2 \text{ s}^{-1} \text{ mm}^{-4}$ at 1400 °C. The corresponding activation energy was 745 kJ/mol,⁸ which is approximately the same as the activation energy for creep (710–750 kJ/mol in this temperature range). The coincidence of the activation energies is not surprising: both cavitation and oxidation involve redistribution of the same elements of the secondary phases via residual glass. Adding external stress only facilitates redistribution of elements attributed to oxidation and causes a shift of the distribution toward the bulk (see Fig. 14). Solution-precipitation of silicon nitride accompanying S-P redistribution of secondary phases contributes to grain reorientation and small anisotropy contribution. Although the oxidation processes involved in subsurface layer formation need more detail study, the whole range of processes accompanying quasi-plastic deformation in ST 1 can be qualitatively explained within expanded cavitation creep model.

Based on the above analysis, strong size effect and both positive and negative influence of heat treatment in air and nitrogen on creep resistance of ST 1 can be predicted. Despite decrease in elastic properties in Fig. 14, additional devitrification during to short term annealing in nitrogen or even in air (when surface oxidation is still small), would improve creep resistance due to strong dependence on volume content of secondary phases (see Eq. (1)). An excessive pre-oxidation producing large ratio between oxidized and core volumes (e.g., in the samples with

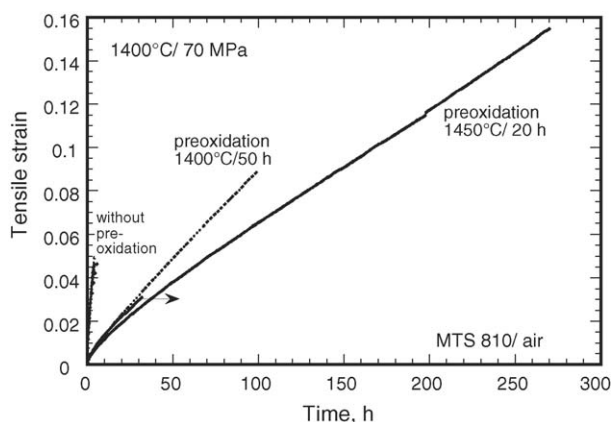


Fig. 15. The demonstration of pre-oxidation effect on creep behavior of ST 1 silicon nitride on large button-head samples. Partial devitrification increases creep resistance whereas large sample size eliminates tertiary like stage due to smaller relative reduction of the load-bearing cross section.

small diameter), would have negative effect on creep resistance. Indeed, both effects have been observed in our earlier study⁸: small samples deformed faster than bigger samples and deleterious effect of the excessive oxidation was more pronounced in smaller samples.⁸ Fig. 15 shows creep curves obtained on modified button-head specimens at identical conditions after different pre-oxidation treatments. Sample without pre-oxidation exhibited repeatedly lifetime of around 4.5–5 h, failure strains of 4.7–5% and strain rates of around $2.6 \times 10^{-6} \text{ s}^{-1}$. Preoxidation at 1400 °C for 50 h caused that the lifetime increased up to 98 h, failure strain up to almost 9% and rate decreased to $2.2 \times 10^{-7} \text{ s}^{-1}$. The effects were even stronger after preoxidation at 1450 °C for 20 h: strain of 15.5% was obtained during 271 h lifetime and strain rate of $1.4 \times 10^{-7} \text{ s}^{-1}$. Note that the accelerated tertiary-like stage is missing in these tests. It is a consequence of the fact that oxide layers were relatively thin compared to sample radius. This simultaneously confirms that one creep mechanism controls creep rate during the whole lifetime.

5. Conclusions

Quasi-plastic creep behavior of a fine-grained silicon nitride with Yb- and Al-based additives accompanied by strong oxidation, cracking of the oxide layers, excessive cavitation at multi-grain junctions and slight texture formation can be explained within the expanded cavitation creep model. High creep rates at temperatures above 1300 °C and failure strains around 20% are facilitated by low viscosity residual glass and small matrix grain size, which enhance all the mechanisms involved in cavitation creep. Instrumented indentation revealed degradation of indentation moduli in the oxide layers and enhanced degradation during creep. Because of the similarities between the mass transport processes in cavitation and oxidation, both creep and oxidation occur simultaneously, though oxidation is enhanced by external stress. Texture formation implied from disappearance of α -silicon nitride and anisotropy of indentation modulus contributes insignificantly (<5%) to total tensile strain. Tertiary-

like creep is attributed to the gradual increase of the applied stress resulting from the reduction of the effective cross section due to the formation of cracked oxide layers.

Acknowledgments

The support for this work provided by Japan Fine Ceramics Centre (Nagoya, Japan), VEGA Grant No. 2/3206/24 (Slovakia) and A. von Humboldt Foundation (Germany) is acknowledged. The help of A. Okada, H. Usami, H. Kawamoto, Y. Ikeda with experimental setup and valuable discussions with W.E. Luecke and S.M. Wiederhorn are highly appreciated.

References

1. Wötting, G., Henricke, J., Feuer, H., Thiemann, K.-H., Vollmer, D., Fechter, E. *et al.*, Reliability and reproducibility of silicon nitride valves: experience and field test. In *Ceramic materials and components for engines*, ed. J. G. Heinrich and F. Aldinger. DKG-Wiley-Vch, Weinheim, Germany, 2001, pp. 181–185.
2. Petzow, G. and Herrmann, M., Silicon nitride ceramics. *Struct. Bond.*, 2002, **102**, 47–167.
3. Abraham, T., Powder market update: nanoceramic applications emerge. *Am. Ceram. Soc. Bull.*, 2004, **83**, 23–25.
4. Wiederhorn, S. M., High temperature deformation of silicon nitride. *Z. Metallkd.*, 2000, **9**, 1053–1058.
5. Melendéz-Martínez, J. J. and Domínguez-Rodríguez, A., Creep of silicon nitride. *Prog. Mater. Sci.*, 2004, **49**, 19–107.
6. Wiederhorn, S. M., Krause Jr., R. F., Lofaj, F. and Täffner, U., Creep behavior of improved high temperature silicon nitride. *Key Eng. Mater.*, 2005, **287**, 381–392.
7. Lofaj, F., Wiederhorn, S. M., Long, G. G., Hockey, B. J., Jemian, P. R., Bowder, L. *et al.*, Non-cavitation tensile creep in silicon nitride with Lu-based additives. *J. Eur. Ceram. Soc.*, 2002, **22**, 2479–2487.
8. Lofaj, F., *Creep behavior and mechanisms in the high performance silicon nitride ceramics*. Dr.Sc. thesis, Institute of Material Research of SAS, Košice, Slovakia, 2004, 128 pp.
9. Hoffmann, M. J., High-temperature properties of Si_3N_4 ceramics. *MRS Bull.*, 1995, 28–32.
10. Thompson, D. P., Sialons: alpha-, beta-, gamma- and beyond. *Silicates Industriels*, 2004, **69**, 1–9.
11. Kondo, N., Wakai, F., Yamagiwa, M., Nishioka, T. and Yamakawa, A., High temperature deformation of silicon nitride ceramics with different microstructures. *Mater. Sci. Eng.*, 1996, **A206**, 45–48.
12. Kondo, N., Suzuki, Y., Miyajima, T. and Ohji, T., High temperature mechanical properties of sinter-forged silicon nitride with ytterbia additive. *J. Eur. Ceram. Soc.*, 2003, **23**, 809–815.
13. Lofaj, F., Usami, H., Ikeda, Y., Mizuta, Y. and Kawamoto, H., Creep fracture behavior of gas pressure sintered silicon nitride by X-ray CT. In *Proceedings of the 1995 Yokohama International Gas Turbine Congress, Vol. 3*, Gas Turbine Society of Japan, Tokyo, Japan, 1995, pp. 37–44.
14. Lofaj, F., Okada, A., Ikeda, Y. and Kawamoto, H., Creep processes in the advanced silicon nitride ceramics. *Key Eng. Mater.*, 2000, **171–174**, 747–754.
15. Lofaj, F., Okada, A. and Kawamoto, H., Tensile creep degradation in quasi-ductile silicon nitride. *Key Eng. Mater.*, 1999, **166**, 95–102.
16. Lofaj, F., Okada, A., Ikeda, Y., Mizuta, Y., Usami, H. and Kawamoto, H., Microstructural degradation accompanying tensile creep deformation in quasi-ductile silicon nitride. *Key Eng. Mater.*, 2000, **175–176**, 321–334.
17. Ferber, M. K. and Jenkins, M. G., Evaluation of the strength and creep-fatigue behavior of hot pressed silicon nitride. *J. Am. Ceram. Soc.*, 1992, **75**, 2453–2462.
18. Wiederhorn, S. M., Hockey, B. J., Cranmer, D. C. and Yeckley, R. Y., Transient creep behaviour of hot isostatically pressed silicon nitride. *J. Mater. Sci.*, 1993, **28**, 445–453.

19. Ohji, T. and Yamauchi, Y., Tensile creep and creep rupture behaviour of monolithic and SiC-whisker reinforced silicon nitride ceramics. *J. Am. Ceram. Soc.*, 1993, **76**, 3105–3112.
20. Gasdaska, Ch. J., Tensile creep in an in situ reinforced silicon nitride. *J. Am. Ceram. Soc.*, 1994, **77**, 2408–2418.
21. Rouxel, T., Wakai, F. and Izaki, K., Tensile ductility of superplastic $\text{Al}_2\text{O}_3\text{-Y}_2\text{O}_3\text{-Si}_3\text{N}_4/\text{SiC}$ composites. *J. Am. Ceram. Soc.*, 1992, **75**, 2363–2372.
22. Evans, A. G., Rice, J. R. and Hirth, J. P., Suppression of cavity formation in ceramics: prospects for superplasticity. *J. Am. Ceram. Soc.*, 1980, **63**, 368–375.
23. Luecke, W. E., Wiederhorn, S. M., Hockey, B. J., Krause Jr., R. F. and Long, G. G., Cavitation contributes substantially to tensile creep in silicon nitride. *J. Am. Ceram. Soc.*, 1995, **78**, 2085–2096.
24. Luecke, W. E. and Wiederhorn, S. M., A new model for tensile creep of silicon nitride. *J. Am. Ceram. Soc.*, 1999, **82**, 2769–2778.
25. Lofaj, F., Blessing, G. V. and Wiederhorn, S. M., Ultrasonic velocity technique for non-destructive quantification of elastic moduli degradation during creep in silicon nitride. *J. Am. Ceram. Soc.*, 2003, **86**, 817–822.
26. Lofaj, F., Smith, D. T., Blessing, G. V., Luecke, W. E. and Wiederhorn, S. M., Instrumented indentation and ultrasonic velocity technique for the evaluation of creep cavitation in silicon nitride. *J. Mater. Sci.*, 2003, **38**, 1403–1412.
27. Lofaj, F., Tensile creep behavior in the advanced silicon nitride. *Mater. Sci. Eng.*, 2000, **A279**, 61–72.
28. Oliver, W. C. and Pharr, G. M., An improved technique for determining hardness and elastic modulus using load and displacement sensing indentation experiments. *J. Mater. Res.*, 1992, **7**, 1564–1583.
29. Kondo, N., Sato, E. and Wakai, F., Geometrical microstructural development in superplastic silicon nitride with rod-shaped grains. *J. Am. Ceram. Soc.*, 1998, **81**, 3221–3227.
30. Lofaj, F., Usami, H., Okada, A. and Kawamoto, H., Long-term creep damage development in a self-reinforced silicon nitride. In *Engineering ceramics '96: higher reliability through processing*, ed. G. N. Babini, M. Haviar and P. Šajgalík. Kluwer Academic Publishers, The Netherlands, 1997, pp. 337–352.
31. Lofaj, F., Usami, H., Okada, A. and Kawamoto, H., Creep damage in an advanced self-reinforced silicon nitride: part I, cavitation in the amorphous phase. *J. Am. Ceram. Soc.*, 1999, **82**, 1009–1019.